

# Strain controlled thermal regulator realized in two-dimensional black and blue phosphorene in-plane heterostructure

Mingyue Xia,<sup>1,2</sup> Luneng Zhao,<sup>1,2</sup> Yuan Chang,<sup>1,2</sup> Hongsheng Liu<sup>①,2</sup>, Gang Zhang,<sup>3,\*</sup> Wuxing Zhou,<sup>4,†</sup> Jijun Zhao,<sup>2,‡</sup> and Junfeng Gao<sup>①,2,§</sup>

<sup>1</sup>State Key Laboratory of Structural Analysis for Industrial Equipment, Dalian University of Technology, Dalian 116024, China

<sup>2</sup>Laboratory of Materials Modification by Laser, Ion and Electron Beams, Ministry of Education, Dalian University of Technology, Dalian 116024, China

<sup>3</sup>Institute of High Performance Computing A\*STAR Singapore 138632, Singapore

<sup>4</sup>School of Materials Science and Engineering, Hunan University of Science and Technology, Xiangtan 411201, China



(Received 16 November 2023; revised 22 February 2024; accepted 23 February 2024; published 7 March 2024)

The reversible phase transition of two-dimensional material allotropes induced by strain engineering has promising applications in nanoelectromechanical systems and memories. Here, we report a series of black and blue phosphorene superlattice (BBPS) can be formed by reversible phase transition between them. The phase transition is with low-energy barrier and can be well regulated by strain engineering, until black phosphorene phase is fully transformed into blue phosphorene phase under strain of  $\varepsilon = 23\%$ . At room temperature, BBPS exhibits a high phase transition rate of about  $10^6$  Hz, which enables reversible phase transition rapidly. Beyond, the unique in-plane heterostructure of BBPS suppresses phonon transmission, lowering thermal conductivity to only 25.6% of black phosphorene. Beyond, nonequilibrium Green's function calculations indicate the thermal conductivity crossing the black-blue phosphorene heterojunction suddenly drops to only 1/3 that of black phosphorene. Therefore, strain engineering can not only achieve reversible phase transition but also modulate the thermal conductivity in very large range, which is excellent in the field of heat flow manipulation and thermal management.

DOI: [10.1103/PhysRevB.109.104106](https://doi.org/10.1103/PhysRevB.109.104106)

## I. INTRODUCTION

Phosphorene is a promising alternative for emerging post-graphene two-dimensional (2D) materials [1,2]. Black phosphorene ( $\alpha$ -P) is a semiconductor with a tunable direct band gap [3–6], large on/off ratios and anisotropic behavior [5,7–12]. Its unique puckered structure results in significant anisotropy in in-plane thermal conductivity, with higher conductivity along the zigzag direction compared to the armchair direction [11,13,14]. Blue phosphorene ( $\beta$ -P), another allotrope of phosphorus, is theorized to have a wider fundamental indirect band gap exceeding 2 eV [15]. And compared to  $\alpha$ -P,  $\beta$ -P demonstrates isotropic behavior. They exhibit extremely distinct electronic properties and thermal properties, but their binding energies are very close, which indicates that the  $\beta$ -P phase is as stable as the  $\alpha$ -P phase [3]. So, it is equally important to explore the synthesis of  $\beta$ -P. Recently, the  $\beta$ -P with a buckled honeycomb structure was successfully prepared by molecular beam epitaxy, which utilizes Au(111), Cu(111), and GaN(001) as substrates [16–21]. Meanwhile, various theoretical investigations of  $\beta$ -P growth mechanisms have been reported. Among them, inducing phase

transition between allotropes serves as an effective strategy to control the growth of  $\beta$ -P [20,22–24], which has attracted great interest in synthesizing high-quality monolayer 2D materials.

Strain engineering is an effective strategy to tune the microstructure and properties of 2D materials. For example, the lattice structures and energies of  $MX_2$  ( $M = \text{Mo}, \text{W}$ ,  $X = \text{S}, \text{Se}, \text{Te}$ ) are very close; the strain can easily induce a reversible phase transition between 2H and 1T' and forms a 2H-1T' superlattice structure [25–31]. Moreover, the 2H-1T' superlattice structure with low contact resistance has been widely used in high-performance field-effect transistors [32]. Similarly, Zhao *et al.* reported that strain can introduce interesting reversibility of the phase transition from  $\beta'$ - $\text{In}_2\text{Se}_3$  to  $\alpha$ - $\text{In}_2\text{Se}_3$ , in which the *in situ* TEM showed a clear  $\beta'$ - $\alpha$  heterojunction superlattice [33,34].

Compared with  $MX_2$  and  $\text{In}_2\text{Se}_3$ , the structures and energies of the phosphorene allotropes are rather close. It has proved that the dislocations introduced in  $\alpha$ -P can flip some specific P atoms from the down to up position, thereby transforming  $\alpha$ -P into  $\beta$ -P [3,4,15]. The black and blue phosphorene superlattice (BBPS) in this process was indeed realized with a low potential barrier for phase transition [35]. Hu *et al.* also found that in-plane strain could transform  $\alpha$ -P phase into  $\beta$ -P phase. The  $\alpha$ -P was extended into the unstable flat hexagonal structure, and then quickly reconstructed into  $\beta$ -P [36]. However, the mechanism of strain-induced phase transition remains unclear.

\* zhangg@ihpc.a-star.edu.sg

† wuxingzhou@hnu.edu.cn

‡ zhaojj@dlut.edu.cn

§ gaojf@dlut.edu.cn

In recent years, a large number of studies have shown that the lattice thermal conductivity can be significantly suppressed or improved under strain [37–41]. Phonon propagation depends on lattice vibration, and the contribution of phonons to thermal transport is related to their own characteristics, such as group velocity, phonon lifetime, harmonic property, etc. These characteristics are related to the bonding state between atoms. Strong bonding strength between atoms often means high group velocity, high phonon lifetime [42]. The more uniform atomic bonding strength means higher phonon harmonic, improving heat transport. Strain engineering can stretch or compress the distance between atoms, thereby regulating the bonding state between atoms and regulating phonon transport performance. Therefore, strain engineering is also an effective means to control the lattice thermal conductivity of materials. For example, Guo shown that the biaxial strain of 4.02% on the monolayer PtSe<sub>2</sub> could reduce the room-temperature lattice thermal conductivity by 60% [39]. Xie *et al.* reported that lattice thermal conductivity of silicene can be increased by seven times in the case of 4% tensile strain [43]. In contrast to PtSe<sub>2</sub> and silicene, the phosphorus atoms in the crystal structure of  $\alpha$ -P and  $\beta$ -P are arranged in two different and parallel planes. It is expected that strain engineering can effectively regulate the lattice thermal conductivity of  $\alpha$ -P and  $\beta$ -P.

In this work, we reveal that black and blue phosphorene superlattice (BBPS) can be self-reconstructed by applying stress in monolayer phosphorene. The stability, strain-induced phase transition, structural evolution barrier, electronic properties, and thermal transport of BBPS are compelling, explored using the density functional theory calculations. Our results indicate the energy difference of the phase transition process is only 3.5 meV. At room temperature, the phase transition rate of up to 10<sup>6</sup> Hz implies that the phase transition is highly sensitive to external effects, and reversible phase transition can easily occur between BBPS. The reversible phase transition of BBPS can greatly reduce thermal conductivity comparing with pure black and blue phosphorene. Our findings not only enrich our understanding of the dynamic process of strain-induced BBPS phase transition, but also pave the way for realizing high-performance adjustable thermal switching by regulating reversible phase transition.

## II. COMPUTATIONAL METHODS

We choose the GGA-PBE and LDA functional in the ground-state geometry optimization and thermal transport property, respectively. As previously reported, GGA functional has more physical components than LDA functional. For the optimization calculation of black phosphorene geometry, the GGA-PBE functional shows better consistency than the LDA functional [44,45]. However, compared with LDA functional, the PBE pseudopotential is too soft for NEGF, and nonphysical imaginary frequencies will appear at the  $\Gamma$  point. Therefore, most calculations of phonon transmission use the LDA functional. But regardless of whether GGA-PBE or LDA is used, the general trend remains unchanged [46]. (See the Supplemental Material [47] for detailed DFT calculations and analysis method of black and blue phosphorene superlattices, also see Refs. [48–61] therein)

The lattice mismatch is extremely low ( $\sim 1.1\%$ ) between zigzag direction of  $\alpha$ -P and  $\beta$ -P. The minimal lattice mismatch facilitates the formation of stable superlattices while minimizing structural defects. As previously defined [59–61], the number of the  $\alpha$ -P and  $\beta$ -P in BBPS is denoted as  $\alpha_m$  and  $\beta_n$  ( $m + n = 8$ ), and its atomic structure is depicted in Fig. 1(a). First, we investigate the energy evolution with  $\alpha$ -P and  $\beta$ -P components in BBPS. When the ratio of  $\alpha$  and  $\beta$  is equal, the relative energy decreases with the increasing of the superlattice width, which is due to the size effect. For example, the relative energy of  $\alpha_1$ - $\beta_1$  is 31 meV/atom higher than that of  $\alpha_4$ - $\beta_4$ , as illustrated in Fig. 1(b). To quantitatively assess the energy loss at the BBPS interface, we explore the effect of the  $\beta$ -P components in BBPS as the  $\beta$ -P components increase from 0–8 keeping the sum of  $\alpha$ -P and  $\beta$ -P components in BBPS ( $m + n = 8$ ) constant. For each BBPS structures, the energy is recorded after full relaxation of the structure. The findings reveal that the maximum relative energy of BBPS exceeds that of  $\alpha$ -P by a mere 3 meV, implying the BBPS is an exceptionally stable structure. Consequently, large-scale fabrication of BBPS may be achievable through strain engineering.

Inspired by the extremely lower relative energy of BBPS and previous studies of the strain-induced phase transition of black phosphorene [36,62–64], we explore the detailed process by which strain-induced  $\alpha$ -P undergoes a series of BBPS evolutions to  $\beta$ -P. As in previous studies, the sum of the  $\alpha$ -P and  $\beta$ -P component is fixed to  $8 = m + n$  in order to quantitatively analyze the regulatory properties of BBPS. We plot the energy of per P atom in BBPS as a function of strain, as shown in Fig. 2. The initial structure used for reference is  $\alpha_8$ - $\beta_0$ , with all strain values relative to it. In particular, only one  $\alpha$ -P component at a time can be transformed into  $\beta$ -P. The  $\alpha$ -P component nearest neighbor to  $\beta$ -P will participate in the next phase transition.

Similar to the previous strain-regulated phosphorous atomic chains phase transition [65], the intersection of the two functions in the phase diagram represents the boundary of the phase transition. Clearly, a stable BBPS structure can be obtained by releasing the in-plane strain. This is because the intersection region corresponds to the tensile and compressive states of the two neighboring phases. For example, when a strain  $\varepsilon = 0.91\%$  is applied to  $\alpha_8$ - $\beta_0$ , the energy-strain curve of  $\alpha_8$ - $\beta_0$  can intersect the that of  $\alpha_7$ - $\beta_1$ . Then the ground state of  $\alpha_7$ - $\beta_1$  is then obtained by fully relaxing the in-plane strain. Following this sequential phase transition path, as strain values reach 4.15%, 6.46%, 6.98%, 11.55%, 13.22%, and 16.59%, the  $\alpha_6$ - $\beta_2$ ,  $\alpha_5$ - $\beta_3$ ,  $\alpha_4$ - $\beta_4$ ,  $\alpha_3$ - $\beta_5$ ,  $\alpha_2$ - $\beta_6$ , and  $\alpha_1$ - $\beta_7$  superlattices will appear accordingly. At an in-plane strain  $\varepsilon = 20.73\%$ , the  $\alpha_1$ - $\beta_7$  structure is anticipated to transition into the  $\alpha_0$ - $\beta_8$  phase. Subsequently, when the strain increased to 23%, the ground state of the  $\beta$ -P phase can be achieved.

Previous studies have demonstrated that when the strain reaches 29%,  $\alpha$ -P transforms into an extremely unstable flat hexagonal structure and then rapidly reconstructs into  $\beta$ -P at low temperatures [36]. Conversely, the transition from the  $\alpha$ -P phase to the  $\beta$ -P phase requires slightly less strain through a localized wavelike process than it does via an overall reorganization. Apart from this,  $\alpha_0$ - $\beta_8$  phase is expected to transform back into  $\alpha_8$ - $\beta_0$  phase when the strain is relaxed. It is similar

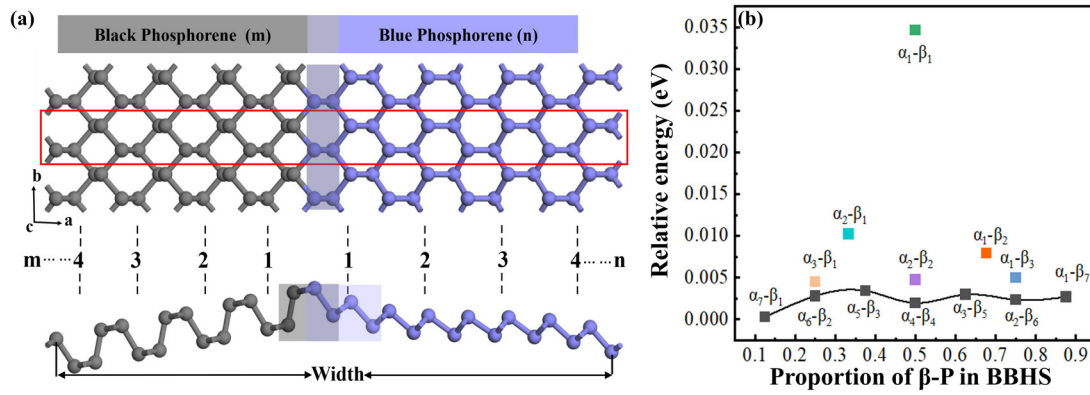


FIG. 1. (a) Schematic diagram of a superlattice constructed from different proportions of blue phosphorene ( $\alpha_m$ ) and blue phosphorene ( $\beta_n$ ), the black and blue atoms represent  $\alpha$ -P and  $\beta$ -P, respectively. The overlap between the black-box region and the blue-box region at the interface is the half-period coshared by  $\alpha$ -P and  $\beta$ -P. (b) The relative energy is the energy difference per P atom of BBPS compared to  $\alpha$ -P of the same size.

to the reversible phase transition processes observed in TMDs [25].

Subsequently, based on the structural stability of black and blue phosphorene superlattice (BBPS) with eight components, we established BBPS structure with 2, 3, 4, 5, 6, and 7 components, respectively. In Fig. S1 [47], we list the relative energies of each component of the BBPS structure. The increase in components will significantly reduce the relative energy of the BBPS. For example, when the ratio of black phosphorene and blue phosphorene is 1:1,  $E_{\alpha_4-\beta_4} > E_{\alpha_3-\beta_3} > E_{\alpha_2-\beta_2} > E_{\alpha_1-\beta_1}$ . When the ratio of black phosphorene and blue phosphorene is 1:3,  $E_{\alpha_2-\beta_6} > E_{\alpha_1-\beta_3}$ . Clearly, their relative energies are different. However, we found that the relative energy differences under the same component are not obvious. The smaller the component, the density of BBPS phase transition points will decrease by strain-induced phase transformation. Likewise, the larger the component, the denser the density of phase transition points. Therefore, the strain-induced gradual phase

transformation from black phosphorene into blue phosphorene is expected to become a universal mode for BBPS with different components.

In the above analysis, we have surprisingly found that strain can controllably induce a reversible phase transition from  $\alpha_8-\beta_0$  to  $\alpha_0-\beta_8$ . In order to further understand the mechanism of reversible phase transition, we conducted in-depth research on the two important factors, namely the energy barrier for phase transition and the phase transition rate. Previous studies have shown that the bond-flipping path (BFP) is the most optimal path of all phase transition paths, leading to lower barrier height for unit cell and supercell [4,35,66,67]. As shown in Fig. 1(b), the energy of BBPS with 32 atoms is very close to that of phosphorene, so we think it can be used as a representative for simulating large-scale phosphorene phase. Figures S2(a)–S2(b) [47] show the unit cell phase transition path and phase transition barrier, which improves the testing accuracy of our calculations.

Next, we explored the energy barrier height for phase transition from  $\alpha_8-\beta_0$  to  $\alpha_7-\beta_1$  along the bond-flipping path in Fig. 3(a) and Fig. 3(c). In particular, the transformation of the  $\alpha$ -P component of  $\alpha_8-\beta_0$  into the  $\beta$ -P component requires overcoming an energy barrier of 1.60 eV, which is only 0.005 eV higher than that of previous report [35]. It confirms that the first energy barrier height for the phase transition of phosphorene along the bond-flipping path is size independent.

During this phase transition step, the structure of  $\alpha_7-\beta_1$  is significantly warped and twisted compared to  $\alpha_8-\beta_0$ . The energy barrier height of  $\alpha_7-\beta_1$  for phase transition to  $\alpha_6-\beta_2$  is reduced by 0.16 eV with respect to the first energy barrier, as shown in Fig. 3(b) and Fig. 3(d). The BBPS phase transition process does not show significant structural deformation in this step. This finding is consistent with previous results and confirms that except for the first phase transition step, the barrier heights of other phase transition step are relatively independent. Although the continuous local bond flipping of the  $\alpha$ -P component in BBPS is relatively independent, it is not completely independent. Similar to the nucleation-diffusion process in experiments [22], the local flipping of  $\alpha$ -P components can cause warping and twisting of the BBPS. Therefore, it is not completely independent. Then, we can estimate the

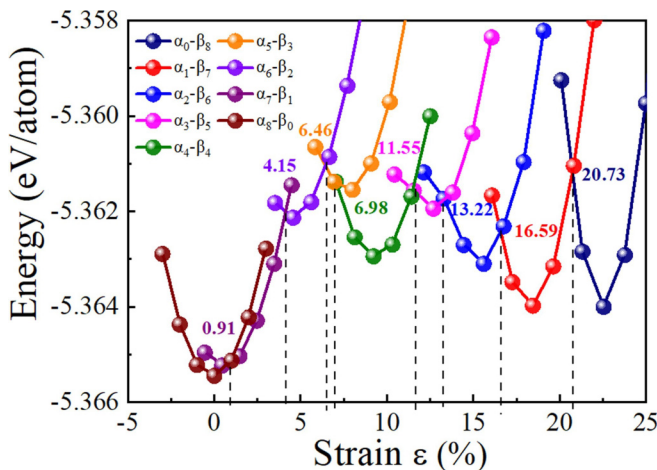


FIG. 2. Phase diagrams are constructed by recording the energy evolution of per P atom during the stretching and compression processes of BBPS compared to  $\alpha_8-\beta_0$ . All strain values are interpreted relative to  $\alpha_8-\beta_0$ . The point of intersection on each colored curve delineates the boundary of phase transition.

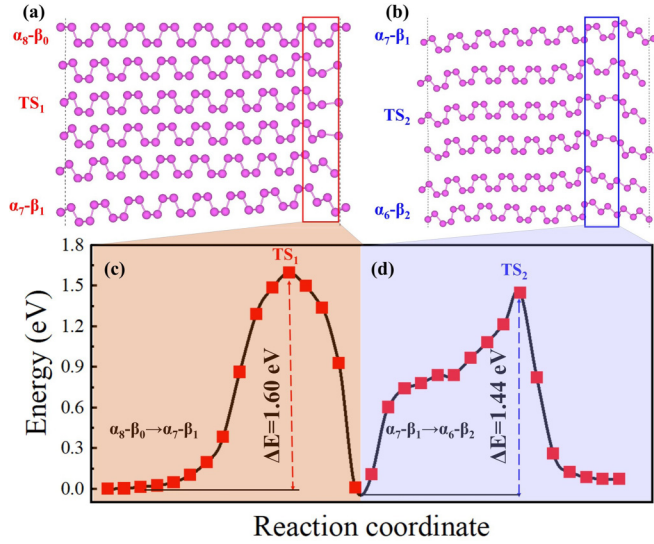


FIG. 3. (a)–(b) Energy change during bonding flipping schematic path for the transition from  $\alpha_8\text{-}\beta_0$  to  $\alpha_7\text{-}\beta_1$  and  $\alpha_7\text{-}\beta_1$  to  $\alpha_6\text{-}\beta_2$ . (c)–(d) Reaction paths of the  $\alpha_8\text{-}\beta_0 \rightarrow \alpha_7\text{-}\beta_1$  and  $\alpha_7\text{-}\beta_1 \rightarrow \alpha_6\text{-}\beta_2$  BBLS phase transitions as a function of the energy barrier.

phase change rate  $R$  as follows [68]:

$$R \sim \left( \frac{k_B T}{h} \right) \times \exp\left( -\frac{\Delta E}{k_B T} \right), \quad (1)$$

where  $T$ ,  $k_B$ , and  $h$  are the temperature, Boltzmann, and Planck constants, respectively.  $\Delta E$  is the phase transition energy barrier of per P atom for both  $\alpha_8\text{-}\beta_0 \rightarrow \alpha_7\text{-}\beta_1$  and  $\alpha_7\text{-}\beta_1 \rightarrow \alpha_6\text{-}\beta_2$ . We show the phase diagrams of the phase transition rate in Figs. 4(a)–4(b). The phase transition frequency of  $\alpha_7\text{-}\beta_1 \rightarrow \alpha_6\text{-}\beta_2$  is slightly faster than that of  $\alpha_8\text{-}\beta_0 \rightarrow \alpha_7\text{-}\beta_1$ , but they are all in the same order of magnitude. It has been reported that phosphorene will thermally decompose up to 673 K, so the temperature range considered in our calculations is 300 K  $\sim$  673 K. At room temperature, the phase change rate  $R$  is approximately  $10^6$  Hz. Besides, the phase transition rate can reach  $10^9$  Hz at the thermal decomposition temperature [68,69], indicating that phase transition can occur in only a few nanoseconds. At the same time, it is proved again that the reversible phase transition of BBPS can be easily adjusted by strain. Consequently, strain can induce reversible phase

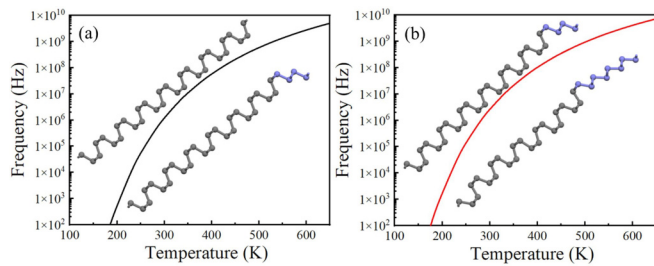


FIG. 4. (a)–(b) Phase diagrams of the  $\alpha_8\text{-}\beta_0$  phase transition to  $\alpha_7\text{-}\beta_1$  and  $\alpha_7\text{-}\beta_1$  phase transition to  $\alpha_6\text{-}\beta_2$  at various temperatures, respectively. The black and blue atoms in the inserts represent  $\alpha\text{-P}$  and  $\beta\text{-P}$ .

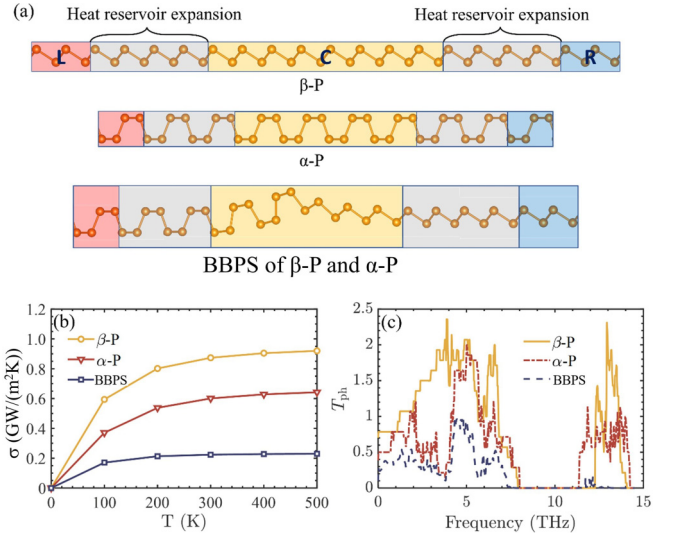


FIG. 5. (a) Model of devices  $\alpha\text{-P}$  and  $\beta\text{-P}$  and BBPS; (b) the thermal conductance and (c) frequency-dependent transmission coefficient curves of devices  $\alpha\text{-P}$  and  $\beta\text{-P}$  and BBPS.

transition in phosphorene and form superlattice heterostructures with varying proportions of coexisting phases.

In order to understand the electronic properties of the BBPS during the phase transition, we calculated the energy band structure of all BBPS and the corresponding charge distribution of the valence band maximum (VBM) and conduction band minimum (CBM) shown on the right-hand side of the energy band structure in Figs. S3(a)–S3(h) [47]. The VBM of the  $\alpha_8\text{-}\beta_0$  derives from bonding orbitals between P atoms in different layers and antibonding orbitals between P atoms in the same layer [70]. However, as shown in Figs. S3(a)–S3(h) [47], the  $\beta\text{-P}$  component in the BBPS can eliminate some of the charge contribution in the VBM. It is presumed that the relative bending of the  $\beta\text{-P}$  configuration during the phase transition may lead to the rearrangement of the charges. Figure S3(i) [47] shows that the charges of VBM and CBM are distributed throughout the space when the  $\beta\text{-P}$  component completely occupies the BBPS. Therefore, the strain applied on BBPS can not only control structural phase transition but also influence its electronic properties.

Due to the phase transition from  $\alpha\text{-P}$  to  $\beta\text{-P}$ , the heterogeneous interface composed of  $\beta\text{-P}$  and  $\alpha\text{-P}$  is inevitably formed in the system. In order to study the effect of heterojunction on heat transport, based on NEGF, we constructed a single heterointerface device composed of  $\beta\text{-P}$  and  $\alpha\text{-P}$  as shown in Fig. 5(a) to study its thermal transport behavior. It is found that the thermal conductance of  $\beta\text{-P}$  is higher than that of  $\alpha\text{-P}$ , but the thermal conductance of BBPS is much lower than that of  $\beta\text{-P}$  [0.87 GW/(m<sup>2</sup>K)] and  $\alpha\text{-P}$  [0.60 GW/(m<sup>2</sup>K)], as shown in Fig. 5(b). At room temperature, compared with  $\beta\text{-P}$  and  $\alpha\text{-P}$ , the thermal conductance of BBPS [0.22 GW/(m<sup>2</sup>K)] decreased by 74.4% and 62.8%, respectively. Note that the thickness of the device of  $\alpha\text{-P}$ ,  $\beta\text{-P}$ , and BBPS are assumed to be the interlayer spacing of  $\alpha\text{-P}$  (0.53 nm) in this work [71]. Through the phonon transmission coefficient curve, it is found that compared with the perfect  $\alpha\text{-P}$  and  $\beta\text{-P}$ , the phonon transmission coefficient of BBPS is suppressed

almost in the whole frequency range. Moreover, the phonons with frequency larger than 7 THz in BBPS structure almost do not participate in thermal transport. In addition, it can be seen from Fig. 5(c) that the transport properties of some low-frequency phonons are suppressed, and low-frequency phonons are the main carriers of thermal transport. Therefore, the thermal transport performance of BBPS is lower than that of  $\alpha$ -P and  $\beta$ -P. This means that the heterogeneous interface formed during the phase transition will significantly reduce the thermal transport performance of  $\alpha$ -P or  $\beta$ -P.

### III. CONCLUSION

In summary, we report that strain tunes the reversible phase transition and thermal transport properties of phosphorene. The phase transition from  $\alpha$ -P to  $\beta$ -P occurs gradually in a wavelike way under strain. According to the results of our phase-transfer-rate-temperature curves, the phase transfer rate at room temperature is as high as  $10^6$  Hz. Therefore, phosphorene can easily undergo a reversible phase transition under strain. Furthermore, strain engineering rearranges the charge distribution of the VBM in BBPS with  $\beta$ -P proportion increasing. Most notably, the transport properties of low-energy

phonons, which are the key factor for thermal transport, are suppressed over almost the entire energy range. This results in a 70% reduction in the thermal transport properties of BBPS compared to intrinsic  $\alpha$ -P and  $\beta$ -P. Therefore, the reversible phase transition also induces a reversible thermal conductivity. Therefore, strain can not only regulate the reversible phase transition of BBPS, but also cause significant reversible thermal conductivity characteristics. The results will enrich the investigation of reversible phase transition and reversible thermal conductivity in 2D materials, which may inspire new applications of different phase superlattice structures of 2D materials in thermofluidic operating systems and phase transition memories.

### ACKNOWLEDGMENTS

This work is supported by the National Natural Science Foundation of China (Grants No. 12374253, No. 12074053, No. 12004064). J.G. thanks the foreign talents in the project (G2022127004L). We also acknowledge computer support from Shanghai Supercomputer Center, DUT supercomputing center, and Tianhe supercomputer of Tianjin center.

The authors declare no conflict of interest.

- 
- [1] L. Kou, C. Chen, and S. C. Smith, *J. Phys. Chem. Lett.* **6**, 2794 (2015).
- [2] J. L. Zhang, C. Han, Z. Hu, L. Wang, L. Liu, A. T. S. Wee, and W. Chen, *Adv. Mater.* **30**, e1802207 (2018).
- [3] J. Guan, Z. Zhu, and D. Tomanek, *Phys. Rev. Lett.* **113**, 046804 (2014).
- [4] Z. Zhu and D. Tomanek, *Phys. Rev. Lett.* **112**, 176802 (2014).
- [5] V. Tran, R. Soklaski, Y. Liang, and L. Yang, *Phys. Rev. B* **89**, 235319 (2014).
- [6] A. Castellanos-Gomez, *J. Phys. Chem. Lett.* **6**, 4280 (2015).
- [7] Z.-Y. Ong, Y. Cai, G. Zhang, and Y.-W. Zhang, *J. Phys. Chem. C* **118**, 25272 (2014).
- [8] Y. Cai, Q. Ke, G. Zhang, Y. P. Feng, V. B. Shenoy, and Y.-W. Zhang, *Adv. Funct. Mater.* **25**, 2230 (2015).
- [9] R. Fei and L. Yang, *Nano Lett.* **14**, 2884 (2014).
- [10] X. Ling, H. Wang, S. Huang, F. Xia, and M. S. Dresselhaus, *Proc. Natl. Acad. Sci. USA* **112**, 4523 (2015).
- [11] G. Qin, Q. B. Yan, Z. Qin, S. Y. Yue, M. Hu, and G. Su, *Phys. Chem. Chem. Phys.* **17**, 4854 (2015).
- [12] X. Wang, A. M. Jones, K. L. Seyler, V. Tran, Y. Jia, H. Zhao, H. Wang, L. Yang, X. Xu, and F. Xia, *Nat. Nanotechnol.* **10**, 517 (2015).
- [13] R. Fei, A. Faghaninia, R. Soklaski, J. A. Yan, C. Lo, and L. Yang, *Nano Lett.* **14**, 6393 (2014).
- [14] Y. Y. Zhang, Q. X. Pei, J. W. Jiang, N. Wei, and Y. W. Zhang, *Nanoscale* **8**, 483 (2016).
- [15] J. Guan, Z. Zhu, and D. Tomanek, *Phys. Rev. Lett.* **113**, 226801 (2014).
- [16] C. Gu, S. Zhao, J. L. Zhang, S. Sun, K. Yuan, Z. Hu, C. Han, Z. Ma, L. Wang, F. Huo, W. Huang, Z. Li, and W. Chen, *ACS Nano* **11**, 4943 (2017).
- [17] E. Goliias, M. Krivenkov, A. Varykhalov, J. Sanchez-Barriga, and O. Rader, *Nano Lett.* **18**, 6672 (2018).
- [18] W. Zhang, H. Enriquez, Y. Tong, A. Bendounan, A. Kara, A. P. Seitsonen, A. J. Mayne, G. Dujardin, and H. Oughaddou, *Small* **14**, e1804066 (2018).
- [19] J. Zhuang, C. Liu, Q. Gao, Y. Liu, H. Feng, X. Xu, J. Wang, J. Zhao, S. X. Dou, Z. Hu, and Y. Du, *ACS Nano* **12**, 5059 (2018).
- [20] J. Zeng, P. Cui, and Z. Zhang, *Phys. Rev. Lett.* **118**, 046101 (2017).
- [21] Y. Kaddar, W. Zhang, H. Enriquez, Y. J. Dappe, A. Bendounan, G. Dujardin, O. Mounkachi, A. El kenz, A. Benyoussef, A. Kara, and H. Oughaddou, *Adv. Funct. Mater.* **33**, 2213664 (2023).
- [22] C. He, S. Xu, X. Dong, C. He, X. Hu, G. Liu, and H. Xu, *Phys. Rev. Mater.* **7**, 034003 (2023).
- [23] A. Kundu, D. Tristant, N. Sheremetyeva, A. Yoshimura, A. Torres Dias, K. S. Hazra, V. Meunier, and P. Puech, *Nano Lett.* **20**, 5929 (2020).
- [24] M. R. K. Musa, C. Zhang, M. Rajapakse, J. B. Jasinski, G. Sumanasekera, and M. Yu, *Phys. Rev. Mater.* **5**, 024007 (2021).
- [25] K. A. Duerloo, Y. Li, and E. J. Reed, *Nat. Commun.* **5**, 4214 (2014).
- [26] K. A. Duerloo and E. J. Reed, *ACS Nano* **10**, 289 (2016).
- [27] S. Song, D. H. Keum, S. Cho, D. Perello, Y. Kim, and Y. H. Lee, *Nano Lett.* **16**, 188 (2016).
- [28] W. Hou, A. Azizimanesh, A. Sewaket, T. Pena, C. Watson, M. Liu, H. Askari, and S. M. Wu, *Nat. Nanotechnol.* **14**, 668 (2019).
- [29] Y. C. Lin, D. O. Dumcenco, Y. S. Huang, and K. Suenaga, *Nat. Nanotechnol.* **9**, 391 (2014).
- [30] W. Li, X. Qian, and J. Li, *Nat. Rev. Mater.* **6**, 829 (2021).

- [31] D. Kim, J. Pandey, J. Jeong, W. Cho, S. Lee, S. Cho, and H. Yang, *Chem. Rev.* **123**, 11230 (2023).
- [32] R. Kappera, D. Voiry, S. E. Yalcin, B. Branch, G. Gupta, A. D. Mohite, and M. Chhowalla, *Nat. Mater.* **13**, 1128 (2014).
- [33] X. Zheng, W. Han, K. Yang, L. W. Wong, C. S. Tsang, K. H. Lai, F. Zheng, T. Yang, S. P. Lau, T. H. Ly, M. Yang, and J. Zhao, *Sci. Adv.* **8**, eabo0773 (2022).
- [34] W. Han, X. Zheng, K. Yang, C. S. Tsang, F. Zheng, L. W. Wong, K. H. Lai, T. Yang, Q. Wei, M. Li, W. F. Io, F. Guo, Y. Cai, N. Wang, J. Hao, S. P. Lau, C. S. Lee, T. H. Ly, M. Yang, and J. Zhao, *Nat. Nanotechnol.* **18**, 55 (2023).
- [35] C. Hogan, P. Lechiffart, S. Brozzesi, S. Voronovich-Solonevich, A. Melnikov, R. Flammini, S. Sanna, and K. Holtgrewe, *Phys. Rev. B* **104**, 245421 (2021).
- [36] T. Hu and J. Dong, *Phys. Rev. B* **92**, 064114 (2015).
- [37] Y. Wu, Z. Chen, P. Nan, F. Xiong, S. Lin, X. Zhang, Y. Chen, L. Chen, B. Ge, and Y. Pei, *Joule* **3**, 1276 (2019).
- [38] C. M. Lin, W. C. Chen, and C. C. Chen, *Phys. Chem. Chem. Phys.* **23**, 18189 (2021).
- [39] S.-D. Guo, *J. Mater. Chem. C* **4**, 9366 (2016).
- [40] C.-W. Wu, X. Ren, S.-Y. Li, Y.-J. Zeng, W.-X. Zhou, and G. Xie, *Appl. Phys. Lett.* **121**, 172201 (2022).
- [41] C.-W. Wu, X. Ren, G. Xie, W.-X. Zhou, G. Zhang, and K.-Q. Chen, *Phys. Rev. Appl.* **18**, 014053 (2022).
- [42] W. G. Zeier, A. Zevalkink, Z. M. Gibbs, G. Hautier, M. G. Kanatzidis, and G. J. Snyder, *Angew. Chem. Int. Ed.* **55**, 6826 (2016).
- [43] H. Xie, T. Ouyang, É. Germaneau, G. Qin, M. Hu, and H. Bao, *Phys. Rev. B* **93**, 075404 (2016).
- [44] S. Kurth, J. P. Perdew, and P. Blaha, *Int. J. Quantum Chem.* **75**, 889 (1999).
- [45] M. Fuchs, J. L. F. Da Silva, C. Stampfl, J. Neugebauer, and M. Scheffler, *Phys. Rev. B* **65**, 245212 (2002).
- [46] M. Arrigoni and G. K. H. Madsen, *Comput. Mater. Sci.* **156**, 354 (2019).
- [47] See Supplemental Material at <http://link.aps.org/supplemental/10.1103/PhysRevB.109.104106> for additional data, including detailed information of DFT calculations and the nonequilibrium Green's function (NEGF) of phonons and thermal transport simulations; energy band structures of  $\alpha$ -P in the BBPS at different occupancies, and the transition process from unit cell  $\alpha$ -P to  $\beta$ -P unit cell. See also Refs. [48–61] therein.
- [48] G. Kresse and J. Furthmüller, *Phys. Rev. B* **54**, 11169 (1996).
- [49] P. E. Blöchl, *Phys. Rev. B* **50**, 17953 (1994).
- [50] J. P. Perdew, K. Burke, and M. Ernzerhof, *Phys. Rev. Lett.* **77**, 3865 (1996).
- [51] M. Yu and D. R. Trinkle, *J. Chem. Phys.* **134**, 064111 (2011).
- [52] T. Yamamoto and K. Watanabe, *Phys. Rev. Lett.* **96**, 255503 (2006).
- [53] C. Caroli, R. Combescot, D. Lederer, P. Nozieres, and D. Saint-James, *J. Phys. C: Solid State Phys.* **4**, 2598 (1971).
- [54] M. Brandbyge, J.-L. Mozos, P. Ordejón, J. Taylor, and K. Stokbro, *Phys. Rev. B* **65**, 165401 (2002).
- [55] A. Fihey, C. Hettich, J. Touzeau, F. Maurel, A. Perrier, C. Köhler, B. Aradi, and T. Frauenheim, *J. Comput. Chem.* **36**, 2075 (2015).
- [56] T. A. Niehaus, M. Elstner, T. Frauenheim, and S. Suhai, *J. Mol. Struct.: THEOCHEM* **541**, 185 (2001).
- [57] M. Elstner, D. Porezag, G. Jungnickel, J. Elsner, M. Haugk, T. Frauenheim, S. Suhai, and G. Seifert, *Phys. Rev. B* **58**, 7260 (1998).
- [58] F. Ersan, D. Kecik, V. O. Özçelik, Y. Kadioglu, O. Ü. Aktürk, E. Durgun, E. Aktürk, and S. Ciraci, *Appl. Phys. Rev.* **6**, 021308 (2019).
- [59] L. Peng, C. Wang, Q. Qian, C. Bi, S. Wang, and Y. Huang, *ACS Appl. Mater. Interfaces* **9**, 40969 (2017).
- [60] Y. Li and F. Ma, *Phys. Chem. Chem. Phys.* **19**, 12466 (2017).
- [61] K. Ren, G. Zhang, L. Zhang, H. Qin, and G. Zhang, *Nanoscale* **15**, 8654 (2023).
- [62] A. S. Rodin, A. Carvalho, and A. H. Castro Neto, *Phys. Rev. Lett.* **112**, 176801 (2014).
- [63] S. Zhang and H. Sun, *Phys. Rev. B* **103**, 155432 (2021).
- [64] Y. Chen, X. Shi, M. Li, Y. Liu, H. Xiao, and X. Chen, *Phys. Chem. Chem. Phys.* **20**, 21832 (2018).
- [65] J. Qiao, L. Zhou, and W. Ji, *Chin. Phys. B* **26**, 036803 (2017).
- [66] D. Zhou, C. Yang, S. Bu, F. Pan, N. Si, P. He, Q. Ji, Y. Lu, and T. Niu, *Phys. Rev. Mater.* **5**, 064002 (2021).
- [67] K. G. Reeves, Y. Yao, and Y. Kanai, *J. Chem. Phys.* **145**, 124705 (2016).
- [68] J. Gao, X. Liu, G. Zhang, and Y. W. Zhang, *Nanoscale* **8**, 17940 (2016).
- [69] X. Liu, J. D. Wood, K. S. Chen, E. Cho, and M. C. Hersam, *J. Phys. Chem. Lett.* **6**, 773 (2015).
- [70] L. Zhang, A. S. Vasenko, J. Zhao, and O. V. Prezhdo, *J. Phys. Chem. Lett.* **10**, 1083 (2019).
- [71] J. Pang, A. Bachmatiuk, Y. Yin, B. Trzebicka, L. Zhao, L. Fu, R. G. Mendes, T. Gemming, Z. Liu, and M. H. Rummeli, *Adv. Energy Mater.* **8**, 1702093 (2018).